# Infra-slow modulation of fast beta/gamma oscillations in the mouse visual system.

Patrycja Orlowska-Feuer[1a*], Annette Elisabeth Allen[2], Timothy Matthew Brown[3], Hanna Jowita Szkudlarek[1b], Robert James Lucas[3], Riccardo Storchi[2*]

**Affiliations:**
[1] Department of Neurophysiology and Chronobiology, Institute of Zoology and Biomedical Research, Jagiellonian University in Krakow, 30-387 Krakow, Poland
[2] Division of Neuroscience and Mental Health, Faculty of Biology, Medicine and Health, University of Manchester, M13 9PT Manchester, UK
[3] Centre for Biological Timing, Faculty of Biology, Medicine and Health, University of Manchester, M13 9PT Manchester, UK
[a] POF present address: Division of Neuroscience and Mental Health, Faculty of Biology, Medicine and Health, University of Manchester, M13 9PT Manchester, UK
[b] HJS present address: Department of Anatomy and Cell Biology, Medical Science Bldg, University of Western Ontario, London, ON, Canada

* Corresponding authors
**Riccardo Storchi, PhD**
riccardo.storchi@manchester.ac.uk
**Patrycja Orlowska-Feuer, PhD**
patrycja.orlowska@uj.edu.pl

**Abbreviated title: Oscillatory activities in the subcortical visual system.**

**Key words:** infra-slow oscillations, beta/gamma oscillations, in vivo electrophysiology, subcortical visual system, photoreceptors

**ABSTRACT**

Infra-slow (<0.02 Hz) and fast beta/gamma (20 – 100 Hz) oscillations in neurophysiological activity have been widely found in the subcortical visual system. While it is well established that fast beta/gamma oscillations are involved in visual processing, the role (if any) of infra-slow oscillations is currently unknown. One possibility is that infra-slow oscillations exert influence by modulating the amplitude of fast oscillations, yet the extent to which these different oscillations arise independently and interact remains unknown. We addressed these questions by recording *in vivo* spontaneous activity from subcortical visual system of visually intact mice, and animals whose retinal network was disrupted by advanced rod/cone degeneration (*rd/rd cl*) or melanopsin loss (*Opn4*$^{-/-}$). We found many neurons expressing only one type of oscillation, and indeed fast oscillations were absent in *rd/rd cl*. Conversely, neurons co-expressing the two oscillations were also common, and were encountered more often than expected by chance in visually intact but not *Opn4*$^{-/-}$ mice. Finally, where they co-occurred we found that beta/gamma amplitude was modulated by the infra-slow rhythm. Our data thus reveal that: 1.) infra-slow and beta-gamma oscillations are separable phenomena; and 2.) that they actively co-occur in a subset of neurones in which the phase of infra-slow oscillations define beta-gamma oscillation amplitude. These findings suggest that infra-slow oscillations could influence vision by modulating beta-gamma oscillations, and raise the possibility that disruptions in these oscillatory behaviours contribute to vision dysfunction in retinal dystrophy.

## KEY POINTS SUMMARY

- Neurophysiological activity in the subcortical visual system fluctuates in both infra-slow and fast oscillatory ranges, however the level of co-occurrence and potential functional interaction of these rhythms is unknown.
- Analyzing dark-adapted spontaneous activity in the mouse subcortical visual system, we find that these two types of oscillation interact uniquely through a population of neurons expressing both rhythms.
- Genetic ablation of rod/cone signaling potentiates infra-slow and abolishes fast beta/gamma oscillations while genetic ablation of melanopsin substantially diminishes the interaction between these two rhythms.
- Our results indicate that in an intact visual system the phase of infra-slow modulates fast beta/gamma oscillations.
- Thus one possible impact of infra-slow oscillations in vision is to guide visual processing by interacting with fast narrowband oscillations.

## INTRODUCTION

Regular infra-slow (<0.02 Hz) oscillations in neurophysiological activity have been found throughout the mammalian visual system, including the retina (Rodieck & Smith, 1966), optic chiasm (Cavaggioni, 1968), the dorsal lateral geniculate nucleus (dLGN) (Albrecht & Gabriel, 1994; Albrecht *et al.*, 1998), ventral lateral geniculate nucleus (vLGN) (Chrobok *et al.*, 2018), olivary pretectal nucleus (OPN) (Szkudlarek *et al.*, 2008, 2012), suprachiasmatic nucleus (SCN) (Aggelopoulos & Meissl, 2000), intergeniculate leaflet (IGL) (Lewandowski *et al.*, 2000, 2002) and primary visual cortex (Filippov & Frolov, 2005). Infra-slow oscillatory rhythm features such as frequency and amplitude are modulated by light and depend on retinal activity (Miller & Fuller, 1992; Albrecht *et al.*, 1998; Lewandowski *et al.*, 2000; Szkudlarek *et al.*, 2012; Orlowska-Feuer *et al.*, 2016*a*). Nevertheless, despite its ubiquity, the contribution of such rhythmicity, if any, to visual processing is still a matter of debate.

Oscillations at a quite different frequency range (20 – 100 Hz, termed beta/gamma) are also a feature of the early visual system. Such oscillations have been implicated in different aspects of visual processing ranging from inter-area communication to feature binding (Gray *et al.*, 1989; Fries, 2005). Recently, we and others also reported that the power of fast beta/gamma oscillations encodes for ambient light intensity and spatially structured changes in luminance (Saleem *et al.*, 2017; Storchi *et al.*, 2017).

Decades of research have highlighted a general organizing principle by which the brain orchestrates oscillations expressed at different timescales. Namely, faster oscillations are "nested" within slower oscillations so that the power of faster oscillations is controlled by the phase of the slower ones. Remarkable example of this phenomenon is the theta-gamma coupling in the hippocampus that has been shown to underlie spatial navigation and object memory recollection (Lisman & Jensen, 2013; Gupta *et al.*, 2016). Electroencephalographic recordings in humans indicates that also infra-slow oscillations can modulate faster rhythms (Vanhatalo *et*

88 *al.*, 2004; Monto *et al.*, 2008). Thus one possible impact of infra-slow oscillations in vision is
89 to guide visual processing by interacting with fast narrowband oscillations.
90 To test this possibility we recorded from mouse subcortical visual system (dLGN, vLGN, and
91 OPN). We found that infra-slow and fast beta/gamma oscillations interact through a population
92 of neurons that co-express both rhythms. Namely in these neurons the phase of infra-slow
93 modulates the amplitude of gamma oscillations. We then asked whether this interaction
94 required intact vision by repeating the same experiments in animals with genetic ablation of
95 rods+cones or melanopsin photoreception. We found that rod+cone loss abolished fast
96 oscillations, but left infra-slow rhythm intact, whereas both oscillations were retained in
97 melanopsin knockouts but their co-expression was substantially reduced. Together these results
98 confirm that infra-slow and fast oscillations are separable phenomena reflecting different
99 network states, and also that in physiological conditions their co-expression in the same neurons
100 is an active consequence of a particular network state that is disrupted by melanopsin loss.

## MATERIALS AND METHODS

*Ethical approval*

All procedures involving animals were carried out in accordance with regulations and standards of the European Community Council Directive of 24 November 1986 (86/609/EEC), approvals of the institutional ethics committee and the UK Home Office and standard and regulations described by (Grundy, 2015).

The following report is in part a re-analysis of previously collected and partially published elsewhere data (Brown *et al.*, 2010; Allen *et al.*, 2011).

*Animals*

Experiments were performed on genetically modified mice which were bred in the animal facility of the Faculty of Life Sciences at Manchester University, UK. Animals were housed under standard conditions (60% of humidity and food and water *at libitum*) with 12:12 h light/dark cycle. Animals were 3 - 5 months old males with three different genetic backgrounds: $Opn1mw^{R}$ mice (C57BL/6:129sv strain) had all types of photoreceptors functional; rodless and coneless (*rd/rd cl)* mice (C3H strain) lacked rods and cones and $Opn4^{-/-}$ mice (C57BL/6:129sv strain) lacked melanopsin. $Opn1mw^{R}$ mice had the medium wavelength-sensitivity (MWS) opsin replaced by human red opsin. This manipulation shifts cone spectral sensitivity but has no other known effects on retinal functions and connectivity (Smallwood *et al.*, 2003; Jacobs & Williams, 2007). Therefore, since the manipulation is inconsequential for this study, $Opn1mw^{R}$ mice were used as 'wild type' animals. All animals were removed from their home cages at the beginning of the projected day and the electrophysiological recordings spanned the mid portion of the day. In total 61 animals were used: 22 of $Opn1mw^{R}$, 22 of $Opn4^{-/-}$ and 17 of *rd/rd cl* mice.

*Surgery*

125 All surgical procedures were conducted under deep urethane anesthesia (1.55 g / kg, 30% w /
126 v; Sigma-Aldrich, Munich, Germany). Animals were injected intraperitoneally and the depth
127 of anesthesia was ascertained by lack of withdrawal and ocular reflexes. If necessary, animals
128 were supplemented with 10% of the initial dose of urethane, however that has never been done
129 during the recordings. Body temperature was automatically maintained at 37 ± 0.5°C by the
130 thermistor with a feedback-controlled heating pad. Anesthetized mice were carefully placed in
131 a stereotaxic frame via ear bars (SR-15M, Narishige International Limited, London, UK). Skin
132 and all soft tissues covering the skull were removed exposing coronal, sagittal and lambdoid
133 sutures. Next, bregma point was determined and craniotomy was performed above the OPN or
134 LGN. The coordinates were assessed based on a stereotaxic brain atlas for mice (Paxinos &
135 Franklin, 2001) and were AP, -2.8; LM, 0.9; DV, -2 to -2.8 mm and AP, -2.5; LM, 2.2; DV, 2.5
136 to 3.5 mm for the OPN and LGN, respectively.

137 *Electrophysiology*

138 A 32-channel multiunit electrode array (A4X8-5 mm-50-200-413; NeuroNexus Technologies,
139 Dallas, TX, USA) was used to record neuronal activities from the pretectum and LGN area. It
140 consisted of 4 silicon shanks (spaced 200 μm), each with 8 recordings sites spaced vertically at
141 50 μm. Neuronal signals were acquired using Recorder64 system (Plexon, Dallas, TX, USA).
142 Signals were amplified (3000×), filtered (300 Hz) and digitized at 40 kHz. All data were saved
143 on a computer hard disc for further analysis.

144 A 4 × 8 electrode array was introduced to a 350 × 600 μm area of the pretectum or LGN and
145 recordings were taken regardless of types of recorded activities (either oscillatory or non-
146 oscillatory). All experiments were conducted in dark adapted conditions provided by coverage
147 of the Faraday cage with light-impermeable material (effective photons flux ~ 9 log photons
148 $cm^{-2}$ $s^{-1}$). Moreover, recordings in some animals were not limited to one penetration.

149 *Histological verification*

150 Prior to the first insertion, the electrode was dipped in fluorescent dye (Cell Tracker CM-Dil,
151 Invitrogen Ltd., UK) in order to verify position of all recording places. At the end of the
152 experiment animals were intracardially perfused with a buffered physiological saline followed
153 by 4% paraformaldehyde in 0.1 M phosphate buffer (pH = 7.2). Brains were removed from the
154 skull and postfixed overnight in the same fixative at 4°C. Cryoprotected brains (immersion in
155 30% sucrose solution for 2-3 days) were cut on a freezing microtome at a coronal plane.
156 Sequential sections (100 µm thick) with CM-Dil depositions were mounted on the gelatin-
157 coated glass slides. Sections were carefully inspected, photographed and ascribed to a related
158 coronal plain of the brain according to the stereotaxic atlas of a mouse brain (Paxinos &
159 Franklin, 2001). Expression of the parvalbumin (calcium binding protein) was used as the
160 marker of OPN neurons (for the precise description of the method see Allen et al., 2011). The
161 optic tract, hippocampus and third ventricle were used as landmarks to determine the LGN
162 borders.

163 *Statistics*

164 *Spike Sorting*

165 Multi-unit recordings were processed using Offline Sorter (version 2.8.8; Plexon) or Spike2
166 (version 6.08). After removal of cross-channel artifacts, each channel was analyzed separately.
167 Single-units were detected and categorized based on spike waveform via principal component
168 analysis (PCA) and related statistic (Fig. 2A-B). Moreover, the inter-spike interval (ISI)
169 histograms were computed to monitor unit refractory period. Cross-correlograms for all isolated
170 units were examined to ensure that each unit was only included once in the further analysis
171 (probability of synchronous firing <0.01). In total we detected 2606 neurons and 2372 (those
172 with firing rates >0.02Hz) were further analysed.

173 *Detection of Infra-Slow activity*

Regular oscillations in the infra-slow range has been previously shown in several publications (Miller & Fuller, 1992; Albrecht & Gabriel, 1994; Lewandowski *et al.*, 2000; Szkudlarek *et al.*, 2008; Orlowska-Feuer *et al.*, 2016*a*; Tsuji *et al.*, 2016; Chrobok *et al.*, 2018). The frequency of those oscillations has been shown to be <0.02 Hz even when long recordings epochs (>1hour, (Orlowska-Feuer *et al.*, 2016*a*; Chrobok *et al.*, 2018)) where considered. However in such works the assessment has been largely done qualitatively based on visual inspection of firing rate time series, autocorrelations and power spectra. Here we devised a procedure to classify those units automatically. We first observed that, for units expressing the most regular infra-slow oscillations, their autocorrelation could be well fit by using the following equation:

$$AC_{fit}(t) = A_1 \cos(2\pi t/T_1)e^{-t/\tau_1} + A_2 \cos(2\pi t/T_2)e^{-t/\tau_2}$$

Where $e^{-t/\tau_i}$ captures the reduction in autocorrelation as function of time lag $t$ and $\cos(2\pi t/T_i)$ captures regular oscillations (Fig.1A-B). The dominant oscillation was defined so that for all units $A_1\tau_1 > A_2\tau_2$. The ratio $T_1/T_2$ clustered around 0.5 and 2 indicating that the second oscillation typically approximates a harmonic of the dominant oscillation (Fig. 1C). For classification we focussed on the dominant oscillation. In order to classify a unit as infra-slow we used the following criteria:

1) Consistent with previous literature the period T1 has to be within the 50s and 450s (Miller & Fuller, 1992; Lewandowski *et al.*, 2000; Filippov *et al.*, 2004; Szkudlarek *et al.*, 2008)

2) The relation $\tau_1/T_1$ between time constant and oscillation period has to be above a fixed threshold (=0.6) in order to reveal regular oscillations (see Fig. 1D-F).

3) The autocorrelation model of equation 1 has to reduce (by >22.5%) the relative fitting error over a simpler model described by $AC_{fit\ simple}(t) = Ae^{-t/\tau}$.

Since no clear indication of bimodality was present in the data (see Fig.1G-H) numerical thresholds for Criteria 2 & 3 were derived empirically to match manual qualitative classification on a subset of data. However the full dataset clearly shows a neat separation between units that

199 were classified as infra-slow and those that were not (Fig.1I). Consistently with results obtained
200 in cat LGN by (Teich *et al.*, 1997) both units classified as infra-slow and those that were not
201 exhibited fluctuations in the infra-slow range (Fig.1J).

202 *Detection of Fast Beta/Gamma activity*

203 We first calculated the Power Spectral Density (PSD) for each unit (Fig.1K) by using the Welch
204 method (time bin = 1s across for whole 900s recording epoch). For this analysis we applied
205 Hamming windows to 512s epochs and 50% overlap between epochs (see MATLAB function
206 *pwelch.m*). In order to identify narrowband peaks in the beta/gamma range we de-trended the
207 PSD by using a one dimensional median filter (Fig.1K; filter order = 20; see MATLAB function
208 *medfilt1.m*). The threshold for a narrowband peaks was then calculated as equalling 5 times the
209 standard deviation of the de-trended PSD (Fig.1K). The units classified as expressing
210 beta/gamma oscillations showed a clear narrow peak in PSD (Fig.1L).

211 *Estimation of Cross-Correlation Index:*

212 A cross-correlation function was estimated between all pairs of units simultaneously recorded.
213 For each pair a cross-correlation index was then obtained by calculating the median of the cross-
214 correlation function in the interval (-10, 10) seconds. To test whether this index was
215 significantly different from zero we applied a sign-test at the distribution of cross-correlation
216 indexes across the selected units.

217 *Estimation of coupling between infra-slow and fast beta/gamma oscillations*

218 Spike timestamps were binned at 1 s for infra-slow and 5 ms for fast beta/gamma to obtain
219 spike counts. Those counts were filtered by using zero-phase Kaiser filters (infra-slow: low-
220 pass filter with cut-off at $2.5/T_1$ Hz and stop-band at $5/T_1$ Hz; fast beta/gamma: band-pass
221 filter with cut-off at 0.8 and 1.2 times the peak frequency and stop-band at 0.6 and 1.4 times).
222 A Hilbert transformation was then applied to the spike counts filtered in the infra-slow range
223 and the phase of these signals was clipped in the range (-π, π). Finally the phase of infra-slow

spike counts was used to divide fast beta/gamma band spike counts into the intervals ((0, π/2); (π/2, π); (0, -π/2); (-π/2, -π)). In order to test against the possibility that the amplitude of fast beta/gamma oscillations is modulated by the phase of infra-slow oscillations we compared the amplitude of these oscillations in the range (-π/2, π/2) with the amplitude observed in the complementary range by using a non-parametric sign-test.

*Permutation Test*

Permutation test was used to test the null hypothesis that occurrence of fast and infra-slow oscillations at the level of individual units were statistically independent events. First we counted the actual number of units expressing both fast and infra-slow rhythms. Then we compared those numbers with a null distribution obtained using the following simple permutation technique. First, for each recording, we generated a binary N-by-2 matrix where each row represented an individual unit, the first column reported presence (or absence) of infra-slow oscillations (presence = 1; absence = 0) and the second column presence (or absence) of fast oscillations. Then, in order to break statistical dependence between these oscillations, we performed a random permutation of one of those columns. Finally, we calculated the number of units co-expressing both rhythms (equivalent to a logical AND). Since different realization of a random permutation can produce different results we estimated the null distribution by repeating this procedure 100000 times. An example is shown in Table 1.

In the real data the firing rate distribution is different between units expressing infra, fast beta/gamma or no oscillations (see Fig. 4G and Fig. 6G). Therefore, the number of units co-expressing infra and fast beta/gamma ($N_{coexpress}$) expected by chance would equal:

$$N_{coexpress} = N \sum_{r=0}^{Rmax} P(beta/gamma\,|R = r)P(Infra|R = r)P(R = r)$$

where $N$ represents the total number of units and $R_{max}$ the maximum firing rate. Thus the random permutation procedure needs to preserve the distributions $P(beta/gamma|R = r)$

and $P(Infra|R = r)$. We implemented this constraint by grouping units into different classes of firing rates and permuting only across units within the same class. Moreover, in order to also exclude confounding effect of different anatomical structures, random permutations were only applied among units recorded from the same structure.

*Statistical Comparisons*

Statistical comparisons of the means ± SD were performed using non-parametrical Mann-Whitney test, Sign-test and Kruskal-Wallis test (followed by Dunn's Multiple Comparison Test). The sampling distribution was verified with Chi-square test. A probability error of $p < 0.05$ was regarded as significant. All data were visualized and statistically examined using GraphPad (version 4.02; GraphPad Software), NeuroExplorer (version 5; Nex Technologies), Statistica software (StatSoft, Inc., Tulsa, Oklahoma, USA) and scripts written in MATLAB (R2019a).

*Codes Accessibility*

The original dataset in .csv format and MATLAB codes for replicating the tests are available online at https://github.com/RStorchi/InfraSlow.

263 **RESULTS**

264 The main aim of this work was to determine the relationship between infra-slow and fast
265 narrowband oscillations in the mouse visual system. We addressed these questions both in
266 image forming and in non-image forming centres in the brain by focussing on the dLGN (image
267 forming), vLGN and OPN (both non-image forming structures).

268

269 *Infra-slow oscillations are widespread in the mouse visual system & co-exist with fast*
270 *narrowband rhythms*

271 Infra-slow oscillations in the subcortical visual system have been observed in many species
272 including rats, cats and monkeys but not previously in mice. Therefore, we first aimed to verify
273 the occurrence of infra-slow oscillatory activity in the spontaneous neuronal firing in the mouse
274 subcortical visual system. We unbiasedly recorded in the absence of visual input (in darkness)
275 from the OPN, dLGN and vLGN in wild type mice.

276 Autocorrelation analysis revealed that ~30% of all recorded units expressed an infra-slow
277 oscillatory rhythm (0.02 – 0.0022 Hz) in spiking activity, resembling previously reported
278 oscillations in the rat subcortical visual system (Albrecht & Gabriel, 1994; Lewandowski *et al.*,
279 2000; Szkudlarek *et al.*, 2008; Chrobok *et al.*, 2018). In Fig.2C-E examples of rhythmically
280 firing units in the dLGN, vLGN and OPN are presented. The mean frequency of observed
281 oscillations ranged between 0.0022 and 0.018 Hz and did not differ between structures
282 (Kruskal-Wallis test, K-W statistics = 0.8394, p = 0.6572; Fig. 2G). The proportion of infra-
283 slow oscillatory neurons was also statistically indistinguishable among these nuclei (28%, 22%
284 and 30% in the dLGN, vLGN and OPN, respectively; Chi-square test, p = 0.3190, Chi-square
285 = 2.285, df = 2, Fig. 3E). In the same dataset described in Fig.2C-G we found that a fraction of
286 neurons expressed fast narrowband oscillations in the beta/gamma range (20 – 100 Hz; Fig. 2H-
287 J). A power spectra density (PSD) analysis and multimodal distribution of peaks at the level of

288 ISI histograms of spontaneous spike activity revealed that 11% (dLGN), 15% (vLGN) and 33%
289 (OPN) of all recorded units expressed such fast oscillations under dark-adapted condition. The
290 frequency of these oscillations averaged at 33.43 ± 10.39 Hz (dLGN), 30.68 ± 6.16 Hz (vLGN)
291 and 34.91 ± 5.09 Hz (OPN). In contrast to infra-slow oscillatory activity, the frequency and
292 proportion of fast oscillating units differed between structures (Kruskal-Wallis test, $p = 0.0271$,
293 K-W statistic = 7.213, Dunn's multiple comparison test; Chi-square test, $p < 0.0001$, Chi-square
294 = 30.29, df = 2; Fig. 2J, Fig. 3E).
295 Based on that data (in total 640 cells from 30 recording sites from 22 wild type animals) we
296 were able to describe four types of spontaneous activity (in darkness) in the sub-cortical visual
297 system of visually intact mice: infra-slow or fast oscillatory activity alone; co-expression of
298 both rhythms; and no oscillatory activity in the above ranges (Fig. 3A-E). Co-expression of
299 infra-slow and fast oscillations were found in 5%, 6% and 15% of all dLGN, vLGN and OPN
300 neurons, respectively (Chi-square test, $p = 0.0022$, Chi-square value = 12.24, df = 2, Fig. 3E).
301 Importantly, all four types of neurons (infra-slow, fast, co-expressing both rhythms and none
302 of them) were found simultaneously in 53% of the recording sessions indicating that their
303 emergence cannot be trivially explained by global fluctuations in neuronal activity (Fig. 3F). In
304 all the structures considered the expression of fast beta/gamma was limited to a minority of
305 units. Simultaneous LFP recordings, reflecting population activity from all units, did not exhibit
306 such narrowband oscillations (Fig. 3G-H).
307 Firing rate of neurons expressing only infra-slow were significantly correlated between each
308 other in all the structures investigated (except the OPN, Table 2 for *Opn1mw*$^{R}$) as revealed by
309 the cross-correlation analysis (see Material and Methods section). Significant correlations were
310 also observed in neurons co-expressing both infra-slow and fast oscillations (Table 2 for
311 *Opn1mw*$^{R}$). Moreover, these two populations were significantly correlated with each other

312 (Table 2 for *Opn1mw*$^{R}$) suggesting that a single infra-slow rhythm coordinates firing rate in both
313 populations.
314
315 *Fast beta/gamma oscillations are modulated in the infra-slow range by diffuse co-expression*
316 *of both rhythms at single unit level*
317 We next aimed to investigate the possibility that infra-slow oscillations modulate fast
318 beta/gamma oscillations. Specifically, we asked how and to what extent the phase of infra-slow
319 oscillations could modulate the amplitude of fast beta/gamma oscillations.
320 We first investigated the possibility that this phenomenon could occur between two distinct
321 neuronal populations, one expressing only infra-slow the other only fast beta/gamma. For each
322 recording and brain structure, we calculated the phase of infra-slow and the amplitude of fast
323 beta/gamma by separately pooling infra-slow and fast beta/gamma units and then by applying
324 a frequency filter and a Hilbert transform to each population (see Methods for details). This
325 analysis revealed that neurons expressing only fast oscillations were largely unaffected by the
326 population-level infra-slow oscillations (Fig. 4A,B). We then asked whether this modulation
327 could instead occur within the same population of neurons. Therefore we repeated the same
328 analysis on populations co-expressing both infra-slow and fast beta gamma oscillations. We
329 found that within these populations fast beta/gamma rhythms were strongly modulated
330 according to the phase of infra-slow oscillations (Fig. 4D,E). These results were consistent
331 across the whole dataset indicating that co-expression of both rhythms at the level of individual
332 unit is required for infra-slow modulation of fast narrowband oscillations (Fig. 4C,F).
333 Finally, we measured the extent to which the expressions of infra-slow and fast oscillations
334 were coordinated at population level.
335 To address this question, we tested the possibility that co-expression of fast and infra-slow
336 oscillations could simply occur by chance. The average firing rate of the four types of neurons

337 were significantly different being highest for units not expressing fast beta/gamma (Fig. 4G;
338 Kruskal-Wallis test, p = 0, n = 822). However the distributions of the four types as function of
339 firing rate were largely overlapping (Fig. 4H) and this allowed us to perform a permutation test
340 that preserved such distributions (see Permutation Test in Methods and Table 1 for details).
341 Therefore we compared the observed number of units where the rhythms were co-expressed
342 with the number we would expect under the null hypothesis that these two oscillations were
343 independent (see Permutation Test in Methods and Table 1 for details). We asked whether a
344 statistical dependence between infra-slow and fast oscillations expressing neurons would
345 emerge from the whole. To do so we pooled together all neuronal groups recorded across
346 structures. We found that the number of neurons co-expressing infra-slow and fast oscillations
347 was larger than expected by chance, indicating that these rhythms tended to co-occur at the
348 level of individual units (Fig. 4I).
349
350 *Outer and inner retina photoreception play different roles in the control of infra-slow*
351 *modulation of fast beta/gamma oscillations*
352 The data from visually intact mice thus suggest that infra-slow and fast oscillations are
353 separable phenomena, which nonetheless co-occur more than expected by chance. Previous
354 results indicate that expression of both infra-slow and fast beta/gamma oscillations depends
355 both on outer and inner retina photoreception (respectively rods/cones and melanopsin)
356 (Orlowska-Feuer *et al.*, 2016*a*; Storchi *et al.*, 2017; Chrobok *et al.*, 2018). We now employed
357 disruption of these two types of photoreceptors to further explore the inter-dependence of
358 oscillations at high and infra-slow frequency. We repeated our initial experiments in a mouse
359 model of aggressive retinal degeneration, lacking rod and cone photoreceptors at the time of
360 recording (*rd/rd cl;* (Lucas & Foster, 1999; Lucas *et al.*, 1999)), and in mice with a more subtle
361 deficit in retinal function caused by loss of the inner retinal photopigment melanopsin (*Opn4*$^{-/-}$

362 ). The detailed analysis of all recorded and analysed cells in all genotypes is presented in Table
363 3. Importantly, there were no differences in the mean firing rates between genotypes across the
364 structures investigated (dLGN: Kruskal-Wallis test, Kruskal-Wallis statistics = 5.901, p =
365 0.0523; vLGN: Kruskal-Wallis test, Kruskal-Wallis statistics = 2.011, p = 0.3659; OPN:
366 Kruskal-Wallis test, Kruskal-Wallis statistics = 5.740, p = 0.0567).
367 In both groups of mice we found significant differences in the prevalence and the features of
368 both infra-slow and fast beta/gamma oscillations compared with visually intact animals. The
369 highest percentage of units expressing infra-slow oscillations was observed in *rd/rd cl* (41%,
370 31% and 56% for the dLGN, vLGN and OPN, respectively), followed by *Opn1mw*$^{R}$ (28%, 22%
371 and 30%), and *Opn4*$^{-/-}$ mice (16%,16% and 18%,). Also the frequency of infra-slow oscillations
372 was significantly different among genotypes. Specifically both *rd/rd cl* and *Opn4*$^{-/-}$ mice
373 exhibited faster infra-slow oscillations compared with visually intact animals, however in the
374 OPN that was only seen as a trend (dLGN: Kruskal-Wallis test, Kruskal-Wallis statistics =
375 37.53, p < 0.0001; vLGN: Kruskal-Wallis test, Kruskal-Wallis statistics = 11.05, p = 0.0040;
376 OPN: Kruskal-Wallis test, Kruskal-Wallis statistics = 3.137, p = 0.2084; Fig. 5).
377 In *rd/rd cl* mice, in which almost half of the recorded units exhibited infra-slow oscillatory
378 activity, fast oscillations were largely abolished (dLGN: 5 out of 258; vLGN: 0 out of 100,
379 OPN: 4 out of 89). On the other hand, in *Opn4*$^{-/-}$ mice the percentage of units expressing fast
380 oscillations was comparable with visually intact animals (7%, 17% and 23% in the dLGN,
381 vLGN and OPN, Fig. 5I). However, the frequency of fast oscillations was altered in *Opn4*$^{-/-}$
382 mice in the OPN (lower in the *Opn4*$^{-/-}$ mice) and vLGN (higher in the *Opn4*$^{-/-}$ mice), but not in
383 dLGN (Fig. 5H).
384 Since both rhythms were retained following melanopsin loss, we next asked whether this
385 manipulation had altered the interaction between infra-slow and fast beta/gamma oscillations.
386 Similarly to what we found in visually intact animals, neurons recorded from *Opn4*$^{-/-}$ mice could

387 be classified into four distinct types on the base of their expression of one or either oscillatory
388 activity. All four types of neurons were found in 28% of recording sites while in 13% of
389 recordings we did not find any oscillatory activity (in total 614 units from 32 recording sites
390 and 22 animals were analysed). Consistently with the *Opn1mw*$^{R}$ genotype, cross-correlation
391 analysis revealed that in the dLGN firing rates were correlated within populations of neurons
392 expressing only infra-slow or both rhythms (Table 2 for *Opn4*$^{-/-}$). However, differently from
393 visually intact animals, the firing rates were not correlated between these two populations
394 (Table 2 for *Opn4*$^{-/-}$). Infra-slow modulation of fast oscillations was observed, but as in visually
395 intact mice, this only occurred in neurons expressing both rhythms (Fig. 6).
396 Finally we asked whether the rate of co-expression of both oscillations was also preserved. We
397 found that this was not the case since co-expression of infra-slow and fast beta/gamma
398 oscillation was not significantly different from chance level in *Opn4*$^{-/-}$ mice (Fig. 6G-I). This
399 result indicates that inner retinal photoreception, while not required for co-existence of both
400 rhythms, is necessary for tying these rhythms together and enabling a diffuse modulation of fast
401 beta/gamma oscillation in the infra-slow range.
402

403 **DISCUSSION**

404 Infra-slow oscillations have been ubiquitously observed in the subcortical visual system,
405 however their function remains poorly understood. Instead fast beta/gamma oscillations are
406 involved in several types of visual processing that include inter-area communication along the
407 visual pathway and feature binding (Gray *et al.*, 1989; Fries, 2005). It was previously shown
408 that gamma rhythm couples with slower rhythms expressed in different brain areas (Vanhatalo
409 *et al.*, 2004; Monto *et al.*, 2008), thus we asked whether that is also the case with infra-slow
410 oscillatory activity in the subcortical visual system.

411 We find that these two types of oscillation are distinct phenomena, but that they do co-occur
412 more than expected by chance. Importantly, this co-occurrence allows the phase of infra-slow
413 oscillations to modulate the amplitude of the fast. These findings reveal a potential mechanism
414 by which infra-slow oscillations could regulate the visual flow – by modulating the amplitude
415 of fast beta/gamma oscillations in the mouse visual system.

416

417 **Infra-slow oscillations are a common feature of subcortical visual systems**

418 Oscillations with the period of minutes were described before in the visual system of adult rats
419 (SCN: Miller & Fuller, 1992; dLGN: Albrecht & Gabriel, 1994; IGL: Lewandowski *et al.*,
420 2000; OPN: Szkudlarek *et al.*, 2008), cats (optic chiasm: Cavaggioni, 1968; retina: Rodieck and
421 Smith, 1966; dLGN: Lorincz *et al.*, 2009, Hughes *et al.*, 2004), rabbits (visual cortex:
422 Aladjalova, 1957), monkeys (visual cortex: Leopold et al., 2003; LGN: Cheong *et al.*, 2011)
423 and mice (prefrontal cortex, EEG recordings: Lecci *et al.*, 2017; prefrontal cortex: Okun *et al.*,
424 2019). Our study is the first to show the existence of infra-slow oscillatory rhythm in the mouse
425 subcortical visual system, where we recorded them in the OPN and in both divisions of LGN.
426 According to the present data, infra-slow oscillatory neurons constitute ~30% of all recorded
427 units in dark adapted mice. The frequency of observed oscillations is slower (~0.005 Hz) than

428 those of rats (~0.01 Hz), however, there is no doubt that the pattern of spike generation is the
429 same (Fig. 2). Differences between these species in their frequency could have different
430 potential origins. On one hand, it could be a genuine species difference in visual physiology.
431 On the other, it may be connected to the fact that albino Wistar rats carry dysfunctions in the
432 visual system (Bolles & Woods, 1964; Lund, 1964; Heiduschka & Schraermeyer, 2008; Nadal-
433 Nicolás *et al.*, 2012) while this study was performed in fully pigmented mice. Finally, it is
434 possible that part of the variability could be simply explained by the small sample sizes used in
435 the previous studies, where single channel recordings were employed as opposed to the higher-
436 yield multichannel electrodes used in this study.
437

438 **Infra-slow and fast beta-gamma oscillations interact through co-expression of both**
439 **rhythms at the level of single units**

440 While co-existence of infra-slow and fast beta/gamma has been reported in the subcortical
441 visual system (Tsuji *et al.*, 2016; Chrobok *et al.*, 2018), until now the extent to which they are
442 independent events and whether they interact was unknown. Our data, obtained by unbiased
443 recordings of all active neurons in the dark, reveal that while a subset of cells express only one
444 type of oscillation, others express either both or none (Fig. 3).
445 In principle, in such population in which not all neurons expressing one type of oscillation also
446 have the other, slow oscillations could still modulate fast beta/gamma oscillations by two types
447 of circuitries. On the one hand, the population of infra-slow neurons could provide a modulation
448 of beta/gamma oscillations, including neurons that did not themselves have infra-slow
449 oscillations (Fig. 7A-F). Alternatively, such modulation could be restricted to neurons in which
450 the two types of oscillations could interact within single neurons (Fig. 7H-J).
451 Our analyses revealed that only neurons co-expressing both oscillations are responsible for
452 mediating infra-slow modulation of fast beta/gamma oscillations (Fig. 4D-F). That is, when

453 they co-occur the amplitude of fast modulations is modified according to the infra-slow rhythm.
454 Importantly, the level of co-expression of these rhythms was higher than expected by two
455 independent events suggesting that the interaction between infra-slow and fast beta/gamma
456 occurs "by design" rather than simply by chance (Fig. 4G).
457 It is currently not possible to map the circuits displayed in Fig.7 onto specific anatomical
458 connections since the infra-slow modulation could be inherited by the retina or generated at the
459 level of the subcortical visual system. Further *in vivo* studies performing simultaneous
460 recordings from optic nerve and from neurons in subcortical visual system would be helpful to
461 clarify the specific circuits involved.
462

463 **Changes to the retinal network alter appearance and interaction of infra-slow and fast**
464 **oscillations**

465 The retina has been previously implicated in the emergence of both infra-slow and fast
466 oscillations in the subcortical brain, with intraocular injection of tetradotoxin abolishing both
467 (Lewandowski & Błasiak, 2004; Szkudlarek *et al.*, 2012; Chrobok *et al.*, 2018). Moreover,
468 selective blockade of phototransduction pathways (classic photoreceptors: rods and cones and
469 melanopsin), as well as, retinal gap junction blockade, were shown to disrupt infra-slow
470 oscillatory rhythm (Orlowska-Feuer *et al.*, 2016*a*, 2016*b*). In all of the cited above data,
471 intraocular injections were performed to assess retina contribution to the generation of infra-
472 slow oscillatory activity in the subcortical visual system. However such approach cannot
473 distinguish between a driving effect, in which infra-slow oscillations in the retina and directly
474 inherited by sub-cortical nuclei, and a gating effect, in which excitation by retina enables
475 subcortical oscillations to emerge. Here, we studied rhythmicity in two mice strains in which
476 the optic nerve was intact and active but in which retinal function was genetically disrupted.
477 These were a model of aggressive photoreceptor degeneration, lacking rod+cone cells (*rd/rd cl*

478 mice), and animals in which inner retina photoreception is ablated (*Opn4*$^{-/-}$ mice). As we were
479 recording activity in the dark, the loss of photoreception in these manipulations is not itself
480 expected to impact our findings, but secondary effects on the retinal circuitry could.
481 Photoreceptors degeneration has knock-on effects on inner-retinal neurons and induces aberrant
482 spontaneous ganglion cell activity in the form of ~10 Hz oscillations (Jones *et al.*, 2003; Ryu
483 *et al.*, 2010; Menzler & Zeck, 2011; Trenholm & Awatramani, 2015), while melanopsin
484 knockout has been reported to impact aspects of retinal development (Renna *et al.*, 2011; Rao
485 *et al.*, 2013; Kirkby & Feller, 2013).
486 Infra-slow oscillations were retained in all genotypes. In fact, they were most prevalent in the
487 *rd/rd cl* (see Table 3), consistent with the simulated effect of reduced retinal input (Zierenberg
488 *et al.*, 2018). Both genetic modifications altered their frequency, and this effect was replicated
489 across all visual centers, consistent with the view that these infra-slow oscillations share a
490 common mechanistic origin.
491 The situation with respect to fast beta/gamma oscillations was quite different, with this behavior
492 essentially absent in *rd/rd cl* mice. This dramatic effect highlights the importance of the retinal
493 activity for this rhythm. Since fast beta/gamma oscillations are typically network phenomena
494 (Buzsáki & Wang, 2012), that could be because the retinal circuits generate these oscillations
495 (Kenyon *et al.*, 2003); that interplay between central and retinal circuits is required to produce
496 this rhythmicity; or that the change in retinal input to the brain alters the activity of central
497 circuits generating this rhythmicity.
498 Perhaps the most interesting alteration in oscillatory activity in transgenic mice was the
499 effective decoupling of infra-slow and fast oscillations in melanopsin knockout animals. While
500 in intact animals these two rhythms co-occurred in individual neurons more often than chance,
501 this property was lost in the *Opn4*$^{-/-}$ genotype. Although we can only speculate as to the change
502 in retinal circuitry responsible for this disruption, it does reinforce the conclusion that the co-

503 occurrence of these oscillations in visually intact animals is an active process. It has been shown
504 that vascular patterning of the retina is dependent upon intact melanopsin photoreception, since
505 this process is disrupted in both dark reared visually intact animals and in animals lacking
506 melanopsin photoreception (Rao *et al.*, 2013). Since vascular patterning affect development of
507 neuronal networks in the retina, this could also affect the coupling between infra-slow and fast
508 narrowband rhythms. This result also provides a new potential mechanism via which this inner
509 retinal photoreceptor typically associated with sub-conscious reflex responses to light could
510 contribute to conventional visual function. While it has been previously shown that the
511 psychophysical threshold of visual sensitivity oscillates in the infra-slow range (Thoss *et al.*,
512 1998) the neuronal mechanism underlying this phenomenon is currently unknown. The reported
513 coupling between infra-slow fluctuation and fast beta/gamma oscillations, the latter being
514 involved in visual processing, points towards such a potential mechanism.
515
516 **Limitations of the study**
517 Since the presented results were obtained from urethane-anesthetized mice an open question is
518 to what extent those results generalize to awake behaving animals. While a number of studies
519 have reported infra-slow and betta/gamma oscillations in various species under different
520 experimental conditions e.g. anesthetics (such as barbiturates, isoflurane) and recording
521 procedures (LFPs, EEG, *in vitro* and *in vivo* neuronal recordings) (Albrecht *et al.*, 1998;
522 Filippov & Frolov, 2005; Hughes *et al.*, 2011; Storchi *et al.*, 2017) some studies have also
523 reported such rhythms in the dLGN and primary visual cortex in behaving animals (Albrecht *et*
524 *al.*, 1998; Filippov & Frolov, 2005; Saleem *et al.*, 2017; Storchi *et al.*, 2017). The frequency of
525 both types of oscillations was higher in freely moving compared to anaesthetized animals
526 (Albrecht *et al.*, 1998; Storchi *et al.*, 2017) and such difference could be due to the specific
527 action of the anesthetics on neurotransmission systems (Hara & Harris, 2002; Wu *et al.*, 2004;

528 Hemmings *et al.*, 2005). Coupling between infra-slow and fast beta/gamma oscillations has also
529 been recorded in awake cortical recordings in human (Monto *et al.*, 2008) but, to the best of our
530 knowledge, never in the subcortical visual structures where our recordings were performed.
531 All recordings in the present study were performed under dark-adapted condition. It has been
532 previously shown that both, infra-slow and beta/gamma oscillatory neurons are modulated by
533 light and visual stimuli. Photopic backgrounds increase mean firing rate but not oscillatory
534 frequency in neurons expressing infra-slow oscillations (Szkudlarek *et al.*, 2012; Chrobok *et*
535 *al.*, 2018, however see also (Albrecht *et al.*, 1998)). In neurons expressing narrowband gamma
536 oscillations both amplitude and frequency of such oscillations are enhanced by steady light
537 (Saleem *et al.*, 2017; Storchi *et al.*, 2017). Those previous results indicate that bright lights
538 strongly increase the expression of fast narrowband oscillations and, consistently with this
539 notion, expression of fast beta/gamma oscillations under dark-adapted conditions is limited to
540 a minority of neurons. While individual units can still express narrowband oscillations such
541 oscillations were not detectable in LFP recordings. This result is in accordance with previous
542 studies indicating that the coupling between LFPs and spikes only becomes apparent with high
543 synchrony at population level (Denker *et al.*, 2011; Storchi *et al.*, 2012). During spontaneous
544 activity, synchrony is strongly reduced in comparison with evoked sensory responses and, as a
545 result, coupling between and between LFP and spikes and between LFPs from different
546 subcortical areas is also reduced (Storchi *et al.*, 2012; Zippo *et al.*, 2013).
547

548 **A potential role for the interaction between infra-slow and fast beta/gamma oscillations**

549 In considering the potential function of these two types of oscillation it is important to
550 remember that they have very different spatiotemporal topology. Infra-slow fluctuations are
551 sustained events that can last minutes/hours and are correlated between different brain areas
552 (Szkudlarek *et al.*, 2008; Chrobok *et al.*, 2018). Infra-slow oscillations have also been closely

553 associated with Resting State Networks (RSNs) observed in human fMRI recordings
554 (Damoiseaux *et al.*, 2006; De Luca *et al.*, 2006; He *et al.*, 2008), and most likely reflect the
555 underlying structural connectivity (Fox & Raichle, 2007; Honey *et al.*, 2007). Fast beta/gamma
556 oscillations typically are short-lasting events that can arise locally and transiently synchronize
557 distant brain areas (Buzsáki, 2006). Those oscillations can be evoked by sensory stimulation
558 (Gray *et al.*, 1989; Cardin *et al.*, 2009; Storchi *et al.*, 2017) or by cognitive tasks (Fries, 2005)
559 but can also emerge spontaneously (Tsuji *et al.*, 2016; Chrobok *et al.*, 2018; Foik *et al.*, 2018).
560 Thus, their spatiotemporal topology is more flexible and need not necessarily reflect the
561 underlying structural connectivity. Accordingly, the interaction between infra-slow and fast
562 beta/gamma could represent a "balancing act" between the opposing needs for transient "on-
563 demand" flexibility – served by fast beta/gamma oscillation – and long-term structural and
564 dynamical stability – served by infra-slow oscillations.
565 Viewed from this perspective, the strong modulation of fast beta/gamma amplitude by infra-
566 slow oscillations observed here could represent a mechanism to oppose runaway plasticity
567 (Abbott & Nelson, 2000) and promote the stability of visual signaling. This control would then
568 be significantly reduced in *Opn4*$^{-/-}$ animals since these two rhythms are independently
569 expressed within the subcortical visual networks. Consistent with this possibility a previous
570 work showed that light modulation of fast beta/gamma oscillations is substantially reduced in
571 *Opn4*$^{-/-}$ animals (Storchi *et al.*, 2017). Thus, although fast beta/gamma could be observed in the
572 dLGN of *Opn4*$^{-/-}$ animals, these oscillations were less controllable by the visual stimulus. This
573 lack in controllability could be due to the lack of the stabilizing action of infra-slow oscillations.

## REFERENCES


Abbott LF & Nelson SB (2000). Synaptic plasticity: taming the beast. *Nat Neurosci* **3,** 1178–1183.

Aggelopoulos NC & Meissl H (2000). Responses of neurones of the rat suprachiasmatic nucleus to retinal illumination under photopic and scotopic conditions. *J Physiol* **523 Pt 1,** 211–222.

Albrecht D & Gabriel S (1994). Very slow oscillations of activity in geniculate neurons of urethane anaesthetized rats. *Neuroreport* **5,** 1909–1912.

Albrecht D, Royl G & Kaneoke Y (1998). Very slow oscillatory activities in lateral geniculate neurons of freely moving and anesthetized rats. *Neurosci Res* **32,** 209–220.

Allen AE, Brown TM & Lucas RJ (2011). A distinct contribution of short-wavelength-sensitive cones to light-evoked activity in the mouse pretectal olivary nucleus. *J Neurosci* **31,** 16833–16843.

Bolles RC & Woods PJ (1964). The ontogeny of behaviour in the albino rat. *Anim Behav* **12,** 427–441.

Brown TM, Gias C, Hatori M, Keding SR, Semo M, Coffey PJ, Gigg J, Piggins HD, Panda S & Lucas RJ (2010). Melanopsin contributions to irradiance coding in the thalamo-cortical visual system. *PLoS Biol*; DOI: 10.1371/journal.pbio.1000558.

Buzsáki G (2006). *Rhythms of the Brain*.

Buzsáki G & Wang X-J (2012). Mechanisms of Gamma Oscillations. *Annu Rev Neurosci* **35,** 203–225.

Cardin JA, Carlén M, Meletis K, Knoblich U, Zhang F, Deisseroth K, Tsai LH & Moore CI (2009). Driving fast-spiking cells induces gamma rhythm and controls sensory responses. *Nature* **459,** 663–667.

Cavaggioni a. (1968). The dark-discharge of the eye in the unrestrained cat. *Pflügers Arch*

*Eur J Physiol* **304,** 75–80.

Cheong SK, Tailby C, Martin PR, Levitte JB & Solomona SG (2011). Slow intrinsic rhythm in the koniocellular visual pathway. *Proc Natl Acad Sci U S A* **108,** 14659–14663.

Chrobok L, Palus-Chramiec K, Jeczmien-Lazur JS, Blasiak T & Lewandowski MH (2018). Gamma and infra-slow oscillations shape neuronal firing in the rat subcortical visual system. *J Physiol* **11,** 2229–2250.

Damoiseaux JS, Rombouts S a. RB, Barkhof F, Scheltens P, Stam CJ, Smith SM & Beckmann CF (2006). Consistent resting-state networks across healthy subjects. *Proc Natl Acad Sci* **103,** 13848–13853.

Denker M, Linde H, Diesmann M, Riehle A & Gru S (2011). The Local Field Potential Reflects Surplus Spike Synchrony. 2681–2695.

Filippov I V. & Frolov VA (2005). Very slow potentials in the lateral geniculate complex and primary visual cortex during different illumination changes in freely moving rats. *Neurosci Lett* **373,** 51–56.

Filippov I V, Williams WC & Frolov V a (2004). Very slow potential oscillations in locus coeruleus and dorsal raphe nucleus under different illumination in freely moving rats. *Neurosci Lett* **363,** 89–93.

Foik AT, Ghazaryan A & Waleszczyk WJ (2018). Oscillations in Spontaneous and Visually Evoked Neuronal Activity in the Superficial Layers of the Cat's Superior Colliculus. *Front Syst Neurosci* **12,** 1–19.

Fox MD & Raichle ME (2007). Spontaneous fluctuations in brain activity observed with functional magnetic resonance imaging. *Nat Rev Neurosci* **8,** 700–711.

Fries P (2005). A mechanism for cognitive dynamics: Neuronal communication through neuronal coherence. *Trends Cogn Sci* **9,** 474–480.

Gray CM, Konig P, Engel AK & Singer W (1989). Oscillatory responses in cat visual cortex

exhibit inter-columnar global stimulus properties. *Nature* **338,** 334–337.

Grundy D (2015). Principles and standards for reporting animal experiments in The Journal of Physiology and Experimental Physiology. *J Physiol* 2547–2549.

Gupta A, van der Meer M, Touretzky D & Redish D (2016). Segmentation of spatial experience by hippocampal theta sequences. *Nat Neurosci* **15,** 1032–1039.

Hara K & Harris A (2002). The Anesthetic Mechanism of Urethane: The Effects on Neurotransmitter-Gated Ion Channels. *Anesth Pharmacol* 313–318.

He BJ, Snyder AZ, Zempel JM, Smyth MD & Raichle ME (2008). Electrophysiological correlates of the brain's intrinsic large-scale functional architecture. *Proc Natl Acad Sci U S A* **105,** 16039–16044.

Heiduschka P & Schraermeyer U (2008). Comparison of visual function in pigmented and albino rats by electroretinography and visual evoked potentials. *Graefe's Arch Clin Exp Ophthalmol* **246,** 1559–1573.

Hemmings HCJ, Akabas MH, Goldstein PA, Trudell JR, Orser BA & Harrison NL (2005). Emerging molecular mechanisms of general anesthetic action. ; DOI: 10.1016/j.tips.2005.08.006.

Honey CJ, Kötter R, Breakspear M & Sporns O (2007). Network structure of cerebral cortex shapes functional connectivity on multiple time scales. *Proc Natl Acad Sci U S A* **104,** 10240–10245.

Hughes SW, Lörincz M, Cope DW, Blethyn KL, Kékesi KA, Parri HR, Juhász G & Crunelli V (2004). Synchronized oscillations at α and θ frequencies in the lateral geniculate nucleus. *Neuron* **42,** 253–268.

Hughes SW, Lőrincz ML, Parri HR & Crunelli V (2011). Infraslow (<0.1Hz) oscillations in thalamic relay nuclei. 145–162.

Jacobs GH & Williams G a (2007). Contributions of the mouse UV photopigment to the ERG

and to vision. *Doc Ophthalmol* **115,** 137–144.

Jones BW, Watt CB, Frederick JM, Baehr W, Chen CK, Levine EM, Milam AH, Lavail MM & Marc RE (2003). Retinal remodeling triggered by photoreceptor degenerations. *J Comp Neurol* **464,** 1–16.

Kenyon GT, Moore B, Jeffs J, Denning KS, Stephens GJ, Travis BJ, George JS, Theiler J & Marshak DW (2003). A model of high-frequency oscillatory potentials in retinal ganglion cells. *Vis Neurosci* **20,** 465–480.

Kirkby L a & Feller MB (2013). Intrinsically photosensitive ganglion cells contribute to plasticity in retinal wave circuits. *Proc Natl Acad Sci U S A* **110,** 12090–12095.

Lecci S, Fernandez LMJ, Weber FD, Cardis R, Chatton JY, Born J & Lüthi A (2017). Coordinated infraslow neural and cardiac oscillations mark fragility and offline periods in mammalian sleep. *Sci Adv*; DOI: 10.1126/sciadv.1602026.

Leopold D a, Murayama Y & Logothetis NK (2003). Very slow activity fluctuations in monkey visual cortex: implications for functional brain imaging. *Cereb Cortex* **13,** 422–433.

Lewandowski MH & Błasiak T (2004). Slow oscillation circuit of the intergeniculate leaflet. *Acta Neurobiol Exp (Wars)* **64,** 277–288.

Lewandowski MH, Błasiak T & Błasiak A (2002). Are ultra-slow isoperiodic oscillations in rat intergeniculate leaflet neurons dependent on reciprocal connection with its contralaterally located counterpart? *Neurosci Lett* **330,** 243–246.

Lewandowski MH, Błasiak T, Domosławski J & Wołkowska a (2000). Ultradian rhythmic neuronal oscillation in the intergeniculate leaflet. *Neuroreport* **11,** 317–321.

Lisman JE & Jensen O (2013). The Theta-Gamma Neural Code. *Neuron* **77,** 1002–1016.

Lorincz ML, Geall F, Bao Y, Crunelli V & Hughes SW (2009). ATP-dependent infra-slow (<0.1 Hz) oscillations in thalamic networks. *PLoS One*; DOI:

674 10.1371/journal.pone.0004447.
675 De Luca M, Beckmann CF, De Stefano N, Matthews PM & Smith SM (2006). fMRI resting
676 state networks define distinct modes of long-distance interactions in the human brain.
677 *Neuroimage* **29,** 1359–1367.
678 Lucas RJ & Foster RG (1999). Neither functional rod photoreceptors nor rod or cone outer
679 segments are required for the photic inhibition of pineal melatonin. *Endocrinology* **140,**
680 1520–1524.
681 Lucas RJ, Freedman MS, Muñoz M, Garcia-Fernández JM & Foster RG (1999). Regulation
682 of the mammalian pineal by non-rod, non-cone, ocular photoreceptors. *Science (80- )*
683 **284,** 505–507.
684 Lund RD (1964). Uncrossed Visual Pathways of Hooded and Albino Rats. *Science (80- )* **149,**
685 1964–1965.
686 Menzler J & Zeck G (2011). Network oscillations in rod-degenerated mouse retinas. *J*
687 *Neurosci* **31,** 2280–2291.
688 Miller JD & Fuller C a (1992). Isoperiodic neuronal activity in suprachiasmatic nucleus of the
689 rat. *Am J Physiol* **263,** R51-8.
690 Monto S, Palva S, Voipio J & Palva JM (2008). Very slow EEG fluctuations predict the
691 dynamics of stimulus detection and oscillation amplitudes in humans. *J Neurosci* **28,**
692 8268–8272.
693 Nadal-Nicolás FM, Jiménez-López M, Salinas-Navarro M, Sobrado-Calvo P, Alburquerque-
694 Béjar JJ, Vidal-Sanz M & Agudo-Barriuso M (2012). Whole Number, Distribution and
695 Co-Expression of Brn3 Transcription Factors in Retinal Ganglion Cells of Adult Albino
696 and Pigmented Rats. *PLoS One*; DOI: 10.1371/journal.pone.0049830.
697 Okun M, Steinmetz NA, Lak A, Dervinis M & Harris KD (2019). Distinct structure of cortical
698 population activity on fast and infraslow timescales. *Cereb Cortex* **29,** 2196–2210.

699 Orlowska-Feuer P, Allen AE, Storchi R, Szkudlarek HJ & Lewandowski MH (2016*a*). The
700 contribution of inner and outer retinal photoreceptors to infra-slow oscillations in the rat
701 olivary pretectal nucleus. *Eur J Neurosci* **43,** 823–833.
702 Orlowska-Feuer P, Jeczmien-Lazur JS, Szkudlarek HJ & Lewandowski MH (2016*b*). Retinal
703 gap junctions are involved in rhythmogenesis of neuronal activity at remote locations –
704 Study on infra-slow oscillations in the rat olivary pretectal nucleus. *Neuroscience* **339,**
705 150–161.
706 Rao S, Chun C, Fan J, Kofron JM, Yang MB, Hegde RS, Ferrara N, Copenhagen DR & Lang
707 RA (2013). A direct and melanopsin-dependent fetal light response regulates mouse eye
708 development. *Nature* **494,** 243–246.
709 Renna J, Weng S & Berson D (2011). Light acts through melanopsin to alter retinal waves
710 and segregation of retinogeniculate afferents. *Nat Neurosci* **14,** 827–829.
711 Rodieck R & Smith P (1966). Slow dark discharge rhythms of cat retinal ganglion cells. *J*
712 *Neurophysiol*. Available at: http://jn.physiology.org/content/jn/29/5/942.full.pdf
713 [Accessed July 6, 2014].
714 Ryu SB, Ye JH, Goo YS, Kim CH & Kim KH (2010). Temporal response properties of retinal
715 ganglion cells in rd1 mice evoked by amplitude-modulated electrical pulse trains.
716 *Investig Ophthalmol Vis Sci* **51,** 6762–6769.
717 Saleem AB, Lien AD, Krumin M, Haider B, Rosón MR, Ayaz A, Reinhold K, Busse L,
718 Carandini M, Harris KD & Carandini M (2017). Subcortical Source and Modulation of
719 the Narrowband Gamma Oscillation in Mouse Visual Cortex. *Neuron* **93,** 315–322.
720 Smallwood PM, Olveczky BP, Williams GL, Jacobs GH, Reese BE, Meister M & Nathans J
721 (2003). Genetically engineered mice with an additional class of cone photoreceptors:
722 implications for the evolution of color vision. *Proc Natl Acad Sci U S A* **100,** 11706–
723 11711.

Storchi R, Bedford RA, Martial FP, Allen AE, Wynne J, Montemurro MA, Petersen RS & Lucas RJ (2017). Modulation of Fast Narrowband Oscillations in the Mouse Retina and dLGN According to Background Light Intensity. *Neuron* **93,** 299–307.

Storchi R, Zippo AG, Caramenti GC, Valente M & Biella GEM (2012). Predicting Spike Occurrence and Neuronal Responsiveness from LFPs in Primary Somatosensory Cortex. ; DOI: 10.1371/journal.pone.0035850.

Szkudlarek HJ, Herdzina O & Lewandowski MH (2008). Ultra-slow oscillatory neuronal activity in the rat olivary pretectal nucleus: comparison with oscillations within the intergeniculate leaflet. *Eur J Neurosci* **27,** 2657–2664.

Szkudlarek HJ, Orlowska P & Lewandowski MH (2012). Light-induced responses of slow oscillatory neurons of the rat olivary pretectal nucleus. *PLoS One* **7,** e33083.

Teich MC, Heneghan C, Lowen SB, Ozaki T & Kaplan E (1997). Fractal character of the neural spike train in the visual system of the cat. *J Opt Soc Am A* **14,** 529–545.

Thoss F, Bartsch B & Stebel J (1998). Analysis of oscillations of the visual sensitivity. *Vision Res* **38,** 139–142.

Trenholm S & Awatramani GB (2015). Origins of spontaneous activity in the degenerating retina. *Front Cell Neurosci* **9,** 1–7.

Tsuji T, Tsuji C, Ludwig M & Leng G (2016). The rat suprachiasmatic nucleus: the master clock ticks at 30 Hz. *J Physiol* **594,** 3629–3650.

Vanhatalo S, Palva JM, Holmes MD, Miller JW, Voipio J & Kaila K (2004). Infraslow oscillations modulate excitability and interictal epileptic activity in the human cortex during sleep. *Proc Natl Acad Sci U S A* **101,** 5053–5057.

Wu X, Ph D, Sun J, Ph D, Evers AS, Crowder M & Ph D (2004). Isoflurane Inhibits Transmitter Release and the Presynaptic Action Potential. 663–670.

Zierenberg J, Wilting J & Priesemann V (2018). Homeostatic Plasticity and External Input

Shape Neural Network Dynamics. *Phys Rev X* **8,** 31018.

Zippo AG, Storchi R, Nencini S, Caramenti GC, Valente M & Biella EM (2013). Neuronal Functional Connection Graphs among Multiple Areas of the Rat Somatosensory System during Spontaneous and Evoked Activities. ; DOI: 10.1371/journal.pcbi.1003104.

## ADDITIONAL INFORMATION

### Data availability statement

The data that support the findings of this study are openly available in github at https://github.com/RStorchi/InfraSlow.

### Conflict of interest statement

The authors declare no competing interests.

### Funding

The work of POF was supported by the Bekker Programme implemented by the Polish National Agency for Academic Exchange (NAWA). RS was funded by National Centre for Replacement Refinement and Reduction of Animals in Research (NC3Rs) via a David Sainsbury Fellowship (NC/P001505/1). RJL was funded by The Welcome Trust (Investigator Award 210684/Z/18/Z) and The European Research Council (268970).

### Author contributions

POF, HJS, RJL, RS designed research; POF, AEA, TMB performed research; RS contributed analytic tools; POF, HJS, RS analyzed data; POF, RJL, RS interpreted the results; POF, RJL, RS wrote the paper. All authors have approved the final version of the manuscript and agreed to be accountable for all aspects of the work in ensuring that questions related to the accuracy or integrity of any part of the work are appropriately investigated and resolved. All persons designated as authors qualify for authorship and all those who qualify for authorship are listed.

776 **TABEL LEGEND**

777 **Table 1: Permutation Test.** The original table contains the data where infra-slow and fast
778 oscillatory expression was detected, the co-expression column tags the units where infra-slow
779 and fast oscillations were co-expressed. The total number of those units is reported as TOTAL
780 COEXP. In the permutation table a random permutation has been applied to the fast column
781 resulting in a different number of units co-expressing both rhythms.

782 **Table 2 Cross-correlation between infra-slow oscillatory neurons, neurons co-expressing**
783 **infra-slow and fast oscillations and between these two populations.** Data was analyzed by
784 sign-test; all p-values < 0.0001 were set at 0; n – number of correlated pairs of neurons; bin size
785 = 1 s. OPN – olivary pretectal nucleus, dLGN – dorsal lateral geniculate nucleus, vLGN –
786 ventral lateral geniculate nucleus, *Opn1mw*$^{R}$ – visually intact mice, *Opn4*$^{-/-}$ - animals lacking
787 melanopsin

788 **Table 3**. **Number and proportion of all recorded neurons**. Infra-slow and fast beta/gamma
789 oscillatory activities presented in different structures of the mice subcortical visual system and
790 in different genotypes. Mean number of cells ± SD per recording site are presented in brackets.
791 OPN – olivary pretectal nucleus, LGN – lateral geniculate nucleus, dLGN – dorsal lateral
792 geniculate nucleus, vLGN – ventral lateral geniculate nucleus, *Opn1mw*$^{R}$ – visually intact mice,
793 *rd/rd cl* – animals lacking rods and cones, *Opn4*$^{-/-}$ - animals lacking melanopsin

# TABELS

## Tabel 1

| Original Table | | | | Permutation Table | | | |
|---|---|---|---|---|---|---|---|
| **#unit** | Infra-slow | Fast | Co-expression | **#unit** | Infra-slow | Fast | Co-expression |
| **#1** | 1 | 0 | 0 | **#1** | 1 | 1 | 1 |
| **#2** | 1 | 1 | 1 | **#2** | 1 | 0 | 0 |
| **#3** | 0 | 0 | 0 | **#3** | 0 | 0 | 0 |
| **#4** | 0 | 0 | 0 | **#4** | 0 | 1 | 0 |
| **#5** | 1 | 1 | 1 | **#5** | 1 | 0 | 0 |
| **#6** | 1 | 1 | 1 | **#6** | 1 | 0 | 0 |
| **#7** | 0 | 0 | 0 | **#7** | 0 | 1 | 0 |
| **#8** | 1 | 0 | 0 | **#8** | 1 | 0 | 0 |
| **#9** | 0 | 0 | 0 | **#9** | 0 | 0 | 0 |
| **TOTAL COEXP** | | | 3 | **TOTALCOEXP** | | | 1 |

797 **Table 2**

| **Structure** | **Infra-slow oscillations** | | | **Co-expressed infra-slow and fast oscillations** | | | **Between** | | |
|---|---|---|---|---|---|---|---|---|---|
| *Opn1mw*$^{R}$ mice | | | | | | | | | |
| | n | p-value | r | n | p-value | r | n | p-value | r |
| dLGN | 420 | 0 | 0.238 | 27 | 0 | 0.370 | 82 | 0 | 0.187 |
| vLGN | 40 | 0 | 0.159 | 11 | 0.065 | 0.106 | 7 | 0.5 | -0.162 |
| OPN | 27 | 0.442 | 0.098 | 32 | 0 | 0.283 | 67 | 0.0002 | 0.118 |
| Pretectum | 45 | 0.036 | 0.086 | 4 | 0.125 | 0.127 | 7 | 1 | -0.0005 |
| *Opn4*$^{-/-}$ mice | | | | | | | | | |
| dLGN | 89 | 0.0003 | 0.107 | 6 | 0.0312 | 0.310 | --- | --- | --- |
| vLGN | 37 | 0.099 | 0.096 | 5 | 0.375 | 0.213 | 21 | 1 | 0.079 |
| OPN | 15 | 0.001 | 0.090 | 6 | 0.031 | 0.306 | --- | --- | --- |
| Pretectum | 33 | 1 | 0.042 | --- | ---- | | --- | --- | --- |

798

799 **Table 3**

| | No. of cells | | | No. of infra-slow oscillatory cells | | | No. of fast oscillatory cells | | |
|---|---|---|---|---|---|---|---|---|---|
| Genotype | *Opn1mw$^{R}$* | *rd/rd cl* | *Opn4$^{-/-}$* | *Opn1mw$^{R}$* | *rd/rd cl* | *Opn4$^{-/-}$* | *Opn1mw$^{R}$* | *rd/rd cl* | *Opn4$^{-/-}$* |
| dLGN | 400 (17 ± 8) | 258 (23 ± 10) | 340 (16 ± 8) | 111 (5 ± 6) | 107 (10 ± 12) | 53 (3 ± 2) | 44 (2 ± 3) | 5 (0.5 ± 0.8) | 23 (1 ± 2) |
| vLGN | 144 (8 ± 7) | 100 (11 ± 7) | 208 (10 ± 8) | 32 (2 ± 2) | 31 (3 ± 5) | 34 (2 ± 2) | 22 (2 ± 3) | 0 | 36 (2 ± 3) |
| OPN | 96 (14 ± 5) | 97 (10 ± 5) | 66 (9 ± 6) | 29 (4 ± 4) | 53 (5 ± 5) | 12 (2 ± 3) | 33 (5 ± 2) | 4 (0.4 ± 0.7) | 15 (2 ± 3) |
| Pretectum (beyond OPN) | 182 (23 ± 17) | 265 (22 ± 12) | 216 (27 ± 8) | 29 (4 ± 2) | 101 (8 ± 7) | 21 (3 ± 2) | 17 (2 ± 2) | 3 (0.25 ± 0.43) | 14 (2 ± 1) |

**Summary information**

| Genotype | | *Opn1mw$^{R}$* | *rd/rd cl* | *Opn4$^{-/-}$* | Genotype | | *Opn1mw$^{R}$* | *rd/rd cl* | *Opn4$^{-/-}$* |
|---|---|---|---|---|---|---|---|---|---|
| Number of animals | Total | 22 | 17 | 22 | Number of recorded/ analysed cells | Total | 936/822 | 768/720 | 902/830 |
| | OPN | 5 | 8 | 5 | | OPN + beyond | 300/278 | 364/362 | 312/282 |
| | LGN | 17 | 9 | 17 | | LGN | 636/544 | 404/358 | 590/548 |

800

## FIGURE LEGENDS

**Fig. 1 Infra-slow and fast beta/gamma criteria for classification.** A) Firing pattern of a representative unit expressing regular infra-slow oscillations. B) The autocorrelogram (black) for unit in panel A can be fit with a simple model expressed in **equation 1** (blue) and composed of a dominant (red) and a sub-dominat (harmonic, green) component. C) Histogram of the ratio between period of the dominant and sub-dominant component in **equation 1** for the whole dataset (n = 2372). D) Visual representation of the second classification criterion for classifying unit as infra-slow: the ratio $\tau_1/T_1$ between time constant and oscillation period has to be above a fixed threshold (= 0.6). Blue dots represent surrogate units meeting the criterion, grey dots represent units that don't meet the criterion and black dots units located on the boundary. E) Autocorrelogram for the units in panel D. F) Same as panel D for all the units in the dataset (n = 2372). Blue dots indicate units that meet all the three criteria for infra-slow classification. G, H) Histograms for $\tau_1/T_1$ ratio (G) and relative error (H) for all units in the dataset (n = 2372). I) Crosscorrelogram for all units in the dataset (n = 2372). Units classified as infra-slow are displayed at the bottom below the red line. All units are re-ordered according to $T_1$ parameter. J) Fano-factor as function of time window for spike counts for infra-slow units (blue; mean & 0.01-0.99 confidence interval) and for units that do not express regular infra-slow oscillations (black; mean mean & 0.01-0.99 confidence interval). Both groups deviate from a stationary Poisson process (grey line). K) Detection of narrowband oscillations in the beta/gamma range. The PSD for a representative unit (black) is rectified by using a median filter (red). A threshold of 5SD is the applied to the rectified PSD (blue) to detect the narrowband peak. L) PSD for all units in the dataset (n = 2372). Units classified as expressing fast beta/gamma oscillations are displayed at the bottom below the red line. All units are re-ordered according to oscillation frequency (note the narrowband peaks indicated by the red arrow).

825 **Fig. 2 The presence of infra-slow and fast beta/gamma oscillatory activity in the mouse**
826 **subcortical visual system.** A) Representative trace recorded in the dLGN revealing infra-slow
827 oscillatory activity in the dark-adapted spontaneous activity. B) Waveforms were clustered and
828 sorted into units based on principal component analysis (PCA). A schematic representation of
829 the placement of one 4 × 8 electrode (= 32 recording channels) showing the distribution of
830 recorded units in the C) OPN and D) LGN and whether they were oscillatory (color coded). E)
831 Representative firing rate histograms (bin size = 1 s) of spontaneous, dark-adapted activity of
832 infra-slow oscillatory cells in the dLGN, vLGN and OPN (labeled above the histograms, not
833 simultaneously recorded). F) FFT analysis performed for the recordings showed in E) indicating
834 the infra-slow frequencies. G) The mean frequency of infra-slow oscillatory activity in the
835 dLGN, vLGN and OPN does not differ between structures (Kruskal-Wallis test, K-W statistics
836 = 0.8394, p = 0.6572). H) Fast beta/gamma oscillatory activity confirmed by PSD analysis. I)
837 ISI histogram (bin size = 0.001 s) computed to confirm existence of harmonic modes in
838 beta/gamma range. J) The mean frequency of fast (beta/gamma) oscillatory activity in the
839 dLGN, vLGN and OPN differs between structures (Kruskal-Wallis test, K-W statistics = 7.213,
840 p = 0.0271, Dunn's multiple comparison test).
841 **Fig. 3 Types of spontaneous activity in the subcortical visual system**. A) Representative
842 firing rate histograms (bin size = 1 s) of spontaneous, dark-adapted activity of simultaneously
843 recorded different types of oscillatory cells in the dLGN. B) FFT and C) PSD analysis were
844 performed to classify cells as infra-slow, fast beta/gamma oscillatory, co-expressing both or
845 none of the above frequencies. D) ISI histograms (bin size = 0.001 s) were computed to confirm
846 existence of harmonic modes in beta/gamma range. E) Venn diagrams showing proportion of
847 four different types of cells recorded in each structure. F) Pie chart summarizing proportion of
848 recording sites (n = 30) in which infra-slow, fast, co-expressed oscillations or none of them
849 were observed. G) PSD for LFPs (left) and for an individual unit (right) recorded from the same

850 recording channel. Note that while a narrowband oscillation is clearly detectable from the
851 spiking activity of the unit no clear narrowband peak can be observed in LFPs. H) Same as
852 panel (G) but for a different recording channel during the same experimental session.

853 **Fig. 4 Infra-slow modulation of fast beta/gamma oscillations in the subcortical visual**
854 **system of *Opn1mw$^R$* mice.** Representative example of simultaneously recorded activity from
855 two separate pools of neurons. Firing rate activity has been filtered in the A) infra-slow and B)
856 fast beta/gamma range and normalized as z-score. The color of the lines denote four different
857 phases of the infra-slow rhythm according to the phase quadrants (dark blue: -π to -π/2 radians;
858 dark red: -π/2 to 0 radians; dim red 0 to π/2 radians; dim blue: π/2 to π radians). C) A non-
859 parametric sign-test comparison between fast beta/gamma amplitude recorded during the "red"
860 vs the "blue" phases shows no significant phase modulation. Here the data are grouped across
861 all experiments in which distinct neuronal pools expressing either infra-slow or fast beta/gamma
862 were simultaneously identified. D) and E) are the same as A) and B), respectively, but for a
863 representative example in which a pool of simultaneously recorded neurons co-expressed both
864 infra-slow and fast oscillations. F) Same as panel C but for all experiments in which a
865 population of neurons co-expressing both rhythms was identified. Within these populations the
866 amplitude of fast beta/gamma is significantly modulated by the phase of infra-slow oscillations.
867 G) Firing rates (mean ± SD) for all the four unit types described in **Figure 2A-E** (Kruskal-
868 Wallis test, p=0, n = 822)**.** H) Distribution of firing rates across the four unit types. I) Statistical
869 comparison between the number of neurons co-expressing infra-slow and fast beta/gamma
870 oscillations that we experimentally observed and the theoretical number predicted by the chance
871 levels and based on the overall number of neurons expressing those two rhythms (either
872 separately or jointly). The number of neurons in which infra-slow and fast beta/gamma are co-
873 expressed (the red line) is larger than chance across our dataset. The null distribution (grey

histogram) is obtained by using the permutation test as described in Material and Methods section. * < 0.05; ** < 0.01; *** < 0.001; **** < 0.0001

**Fig. 5 Inner and outer retina contribution to infra-slow and fast beta/gamma oscillatory rhythms emergence.** Representative firing rate histograms (bin size = 1 s) of infra-slow oscillatory activity recorded within the dLGN of A) *Opn1mw*$^{R}$, B) *rd/rd cl* and C) *Opn4*$^{-/-}$ mice. D) Peaks (color coded) correspond to the infra-slow frequency of oscillations presented on A – C, respectively. E) Mean frequency of recorded infra-slow oscillations differs between genotypes in the dLGN and vLGN, but not in the OPN (however the trend could be seen). F) The proportion of infra-slow oscillatory cells differs between the genotypes (Chi-square Test; dLGN: p = 0.0005, Chi-square statistic = 15.40, df = 2; vLGN: p = 0.0400, Chi-square statistic = 6.437, df = 2; OPN: p < 0.0001, Chi-square statistic = 33.32, df = 2). G) Normalized PSDs for two different OPN neurons recorded in *Opn1mw*$^{R}$ and *Opn4*$^{-/-}$ mice (colour coded). H) The mean frequency of fast beta/gamma oscillating neurons differs between *Opn1mw*$^{R}$ and *Opn4*$^{-/-}$ in the OPN and vLGN, but not dLGN. I) The proportion of fast beta/gamma oscillatory cells differs between the genotypes (Chi-square Test: dLGN: p = 0.0381, Chi-square statistic = 6.536, df = 2; vLGN: p = 0.0001, Chi-square statistic = 18.12, df = 2; OPN: p < 0.0001, Chi-square statistic = 28.44, df = 2;=). Please note, that fast oscillatory cells were not recorded at all in vLGN in *rd/rd cl* animals. Data in E analysed by Kruskal-Wallis test followed by Dunn's multiple comparison test; data in H analysed by Mann Whitney. * < 0.05; ** < 0.01; *** < 0.001; **** < 0.0001

**Fig. 6 Infra-slow modulation of fast beta/gamma oscillations in the subcortical visual system of *Opn4*$^{-/-}$ mice.** Same as Figure 4 but for the *Opn4*$^{-/-}$ dataset. * < 0.05; ** < 0.01; *** < 0.001; **** < 0.0001

**Fig. 7 Potential circuits mediating infra-slow modulation of fast beta/gamma oscillations.** A-F) The amplitude of fast/beta gamma oscillations is modulated according to a distinct but

functionally connected population expressing infra-slow oscillations. In this way coherence of oscillations in the beta/gamma range is modulated by the phase of infra-slow oscillations. A-C) Simulated firing pattern of a neuronal population expressing infra-slow oscillations (A) and magnified single units activity at different phase of the infra-slow oscillations (B). The population expresses changes in phase in the infra-slow range (C, top panel) but no fast beta/gamma oscillations (C, bottom panel). (D-F) A second neuronal population lacks infra-slow modulation of firing rate (D) but exhibits epochs of regular fast beta/gamma oscillations (E, bottom) interleaved with epochs lacking such fast rhythms (E, top). The amplitude of fast-beta gamma oscillations is coupled to the phase of infra-slow activity (F). H) Simulated firing of a neuronal population expressing both infra-slow and fast beta/gamma oscillations. I) Magnified single units activity at different phase of the infra-slow oscillations. Clear beta/gamma oscillations can be observed during epochs of high firing rates. J) Within the same population the amplitude of fast-beta gamma oscillations is coupled to the phase of infra-slow activity.

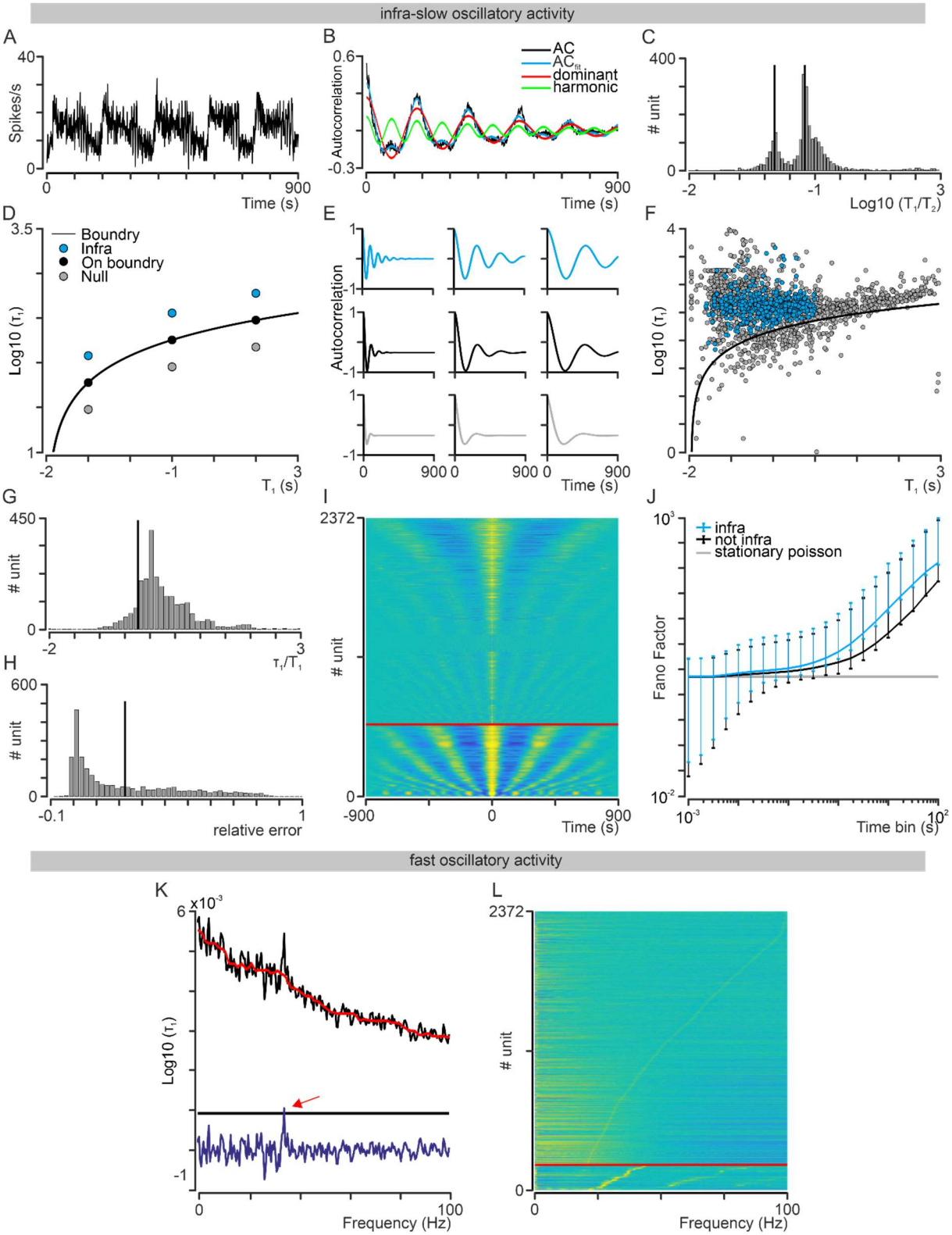
infra-slow oscillatory activity
A
Spikes/s
Time (s)
B
Autocorrelation
AC
AC_fit
dominant
harmonic
Time (s)
C
# unit
Log10 (T1/T2)
D
Boundry
Infra
On boundry
Null
Log10 (τ1)
T1 (s)
E
Autocorrelation
Time (s)
F
Log10 (τ1)
T1 (s)
G
# unit
τ1/T1
H
# unit
relative error
I
# unit
Time (s)
J
infra
not infra
stationary poisson
Fano Factor
Time bin (s)
fast oscillatory activity
K
Log10 (τ1)
Frequency (Hz)
L
# unit
Frequency (Hz)

# Fig. 1

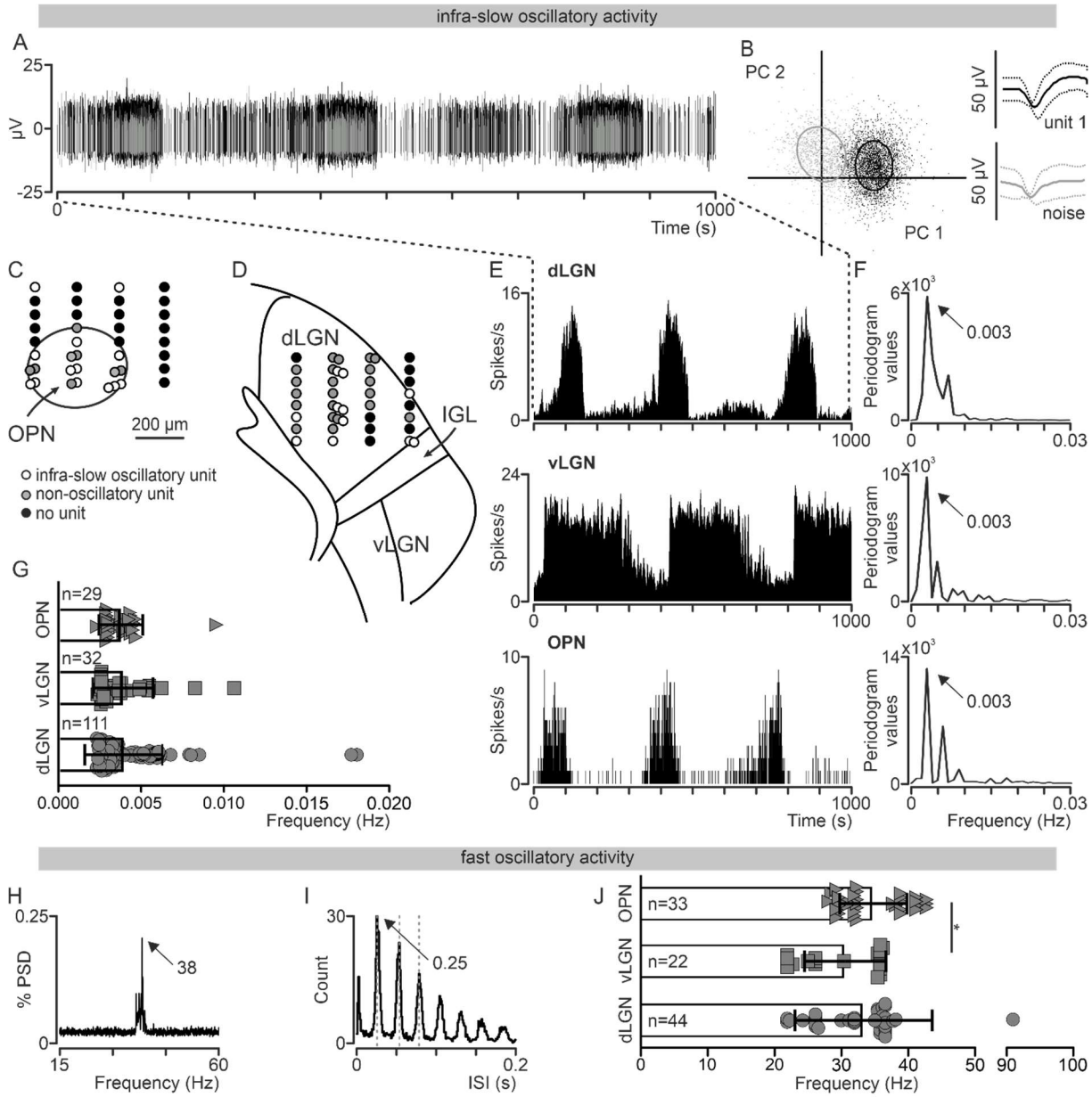
infra-slow oscillatory activity
A
25
μV
0
-25
0
1000
Time (s)
B
PC 2
PC 1
50 μV
unit 1
50 μV
noise
C
OPN
200 μm
infra-slow oscillatory unit
non-oscillatory unit
no unit
D
dLGN
IGL
vLGN
E
dLGN
16
Spikes/s
0
1000
vLGN
24
Spikes/s
0
1000
OPN
10
Spikes/s
0
1000
Time (s)
F
x10³
6
Periodogram values
0.003
0
0.03
Frequency (Hz)
x10³
10
Periodogram values
0.003
0
0.03
x10³
14
Periodogram values
0.003
0
0.03
Frequency (Hz)
G
OPN
n=29
vLGN
n=32
dLGN
n=111
0.000
0.005
0.010
0.015
0.020
Frequency (Hz)
fast oscillatory activity
H
0.25
% PSD
38
0
15
60
Frequency (Hz)
I
30
Count
0.25
0
0
0.2
ISI (s)
J
OPN
n=33
vLGN
n=22
dLGN
n=44
*
0
10
20
30
40
50
90
100
Frequency (Hz)

# Fig. 2

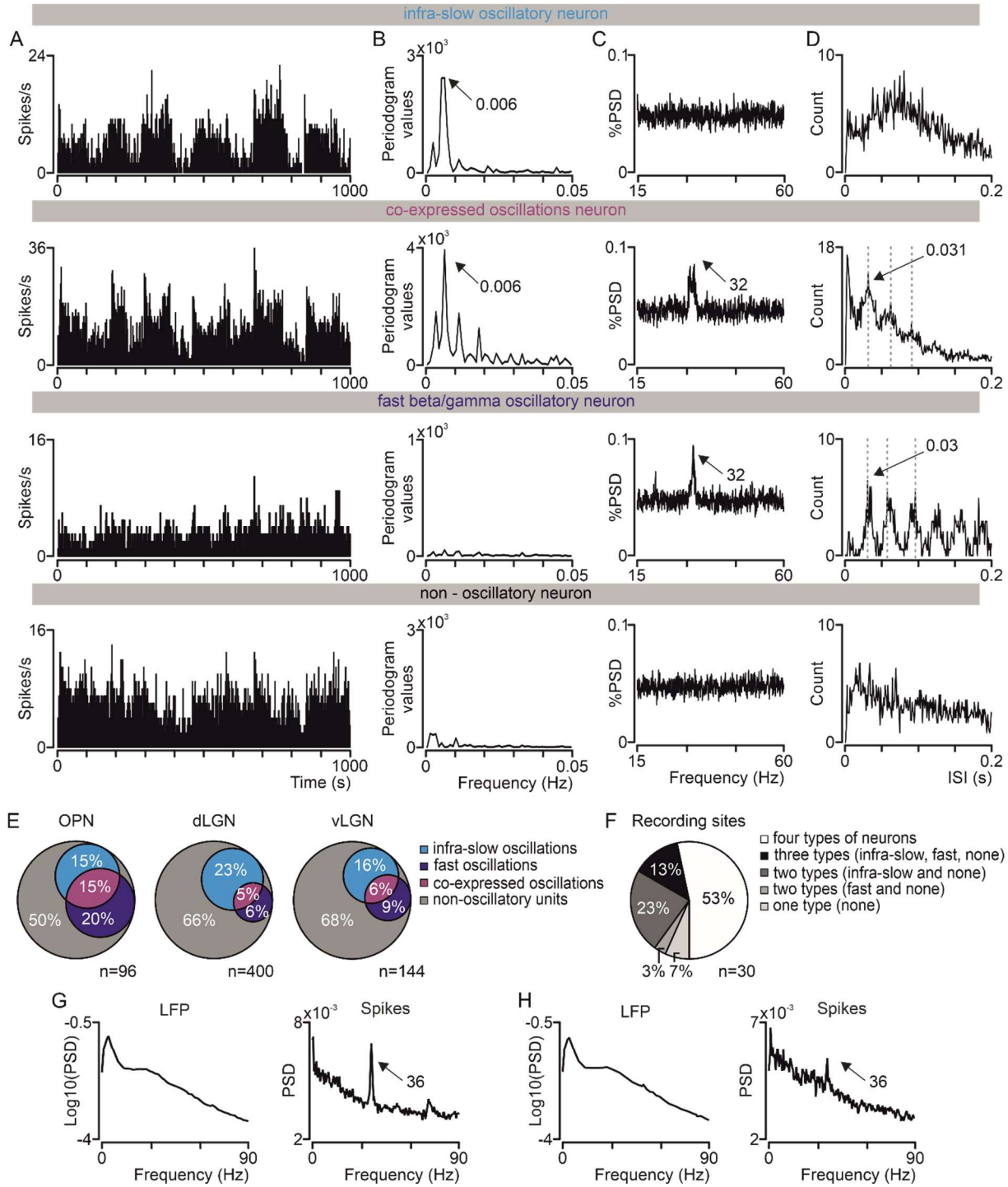
infra-slow oscillatory neuron
co-expressed oscillations neuron
fast beta/gamma oscillatory neuron
non - oscillatory neuron
A
B
C
D
Spikes/s
Periodogram values
%PSD
Count
0.006
32
0.031
0.03
Time (s)
Frequency (Hz)
ISI (s)
E
OPN
dLGN
vLGN
infra-slow oscillations
fast oscillations
co-expressed oscillations
non-oscillatory units
15%
15%
20%
50%
23%
5%
6%
66%
16%
6%
9%
68%
n=96
n=400
n=144
F
Recording sites
four types of neurons
three types (infra-slow, fast, none)
two types (infra-slow and none)
two types (fast and none)
one type (none)
13%
23%
53%
3%
7%
n=30
G
H
LFP
Spikes
Log10(PSD)
PSD
36

# Fig. 3

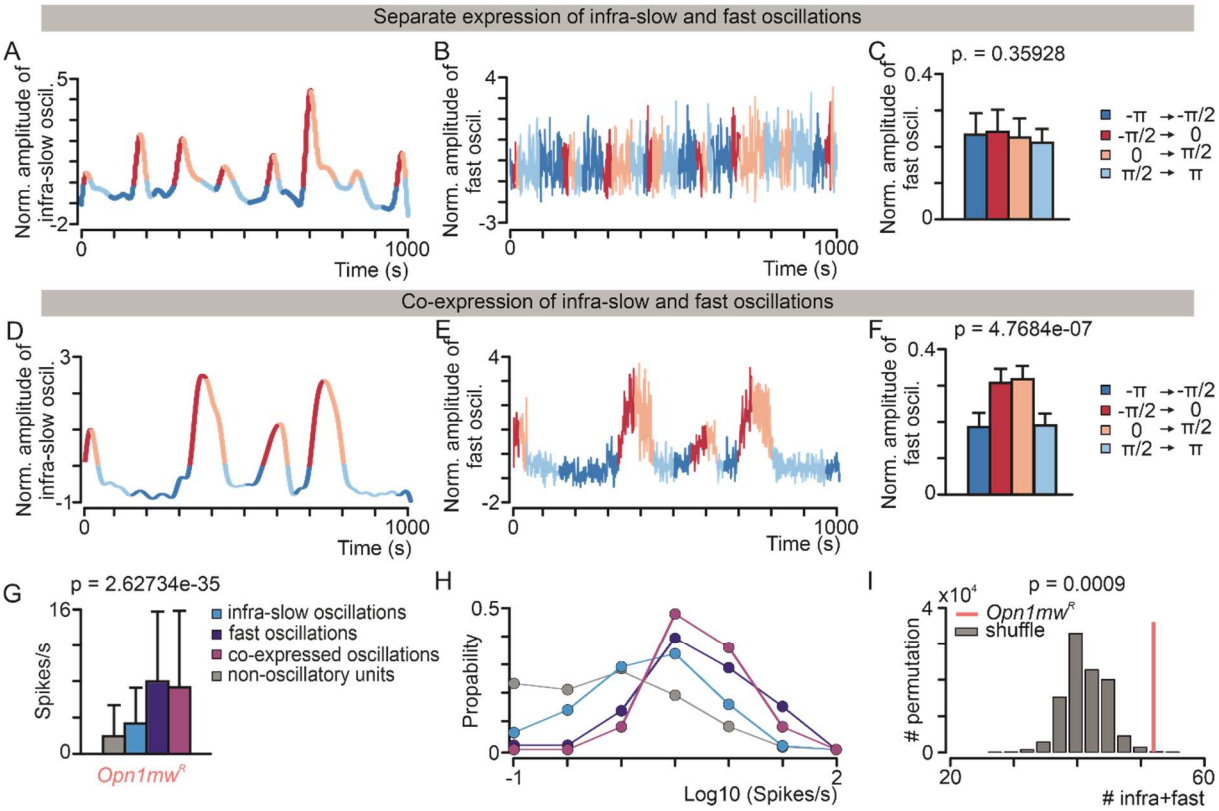
Separate expression of infra-slow and fast oscillations
A
Norm. amplitude of infra-slow oscil.
Time (s)
B
Norm. amplitude of fast oscil.
Time (s)
C
p. = 0.35928
Norm. amplitude of fast oscil.
-π → -π/2
-π/2 → 0
0 → π/2
π/2 → π
Co-expression of infra-slow and fast oscillations
D
Norm. amplitude of infra-slow oscil.
Time (s)
E
Norm. amplitude of fast oscil.
Time (s)
F
p = 4.7684e-07
Norm. amplitude of fast oscil.
-π → -π/2
-π/2 → 0
0 → π/2
π/2 → π
G
p = 2.62734e-35
Spikes/s
infra-slow oscillations
fast oscillations
co-expressed oscillations
non-oscillatory units
Opn1mw^R
H
Propability
Log10 (Spikes/s)
I
p = 0.0009
x10^4
Opn1mw^R
shuffle
# permutation
# infra+fast

# Fig. 4

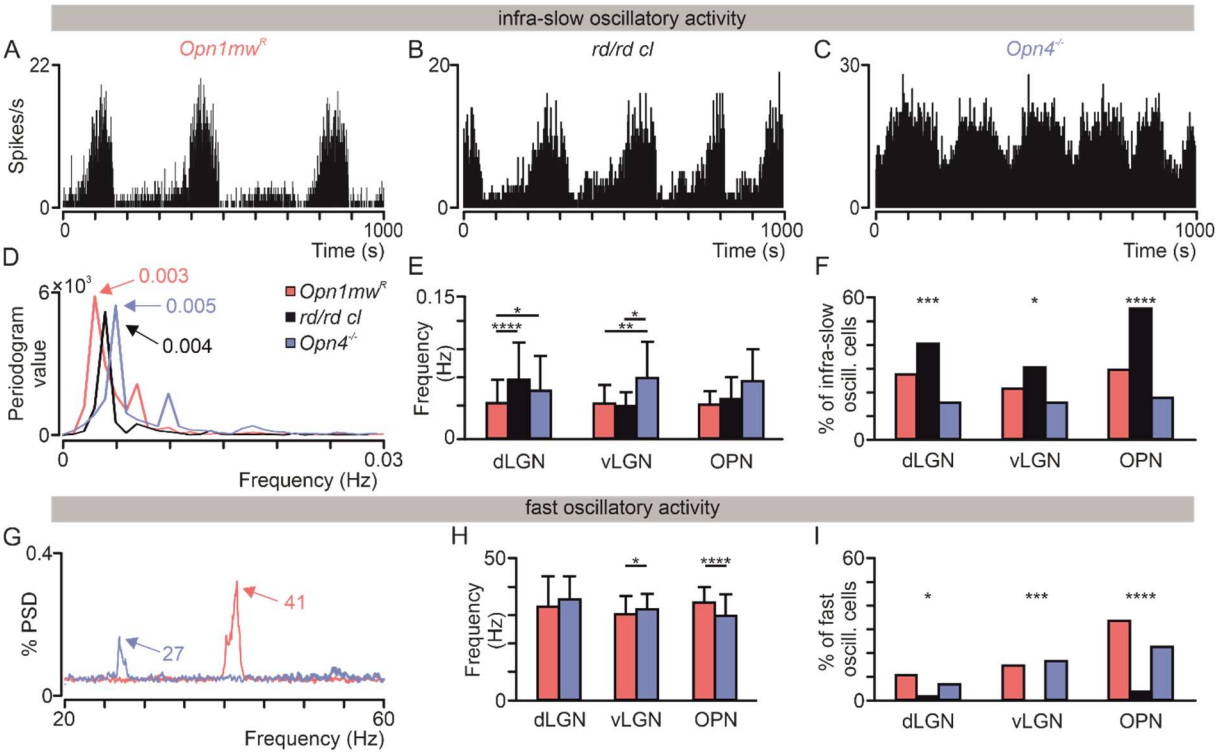
infra-slow oscillatory activity
A
Opn1mw^R
Spikes/s
22
0
0
1000
Time (s)
B
rd/rd cl
20
0
0
1000
Time (s)
C
Opn4^-/-
30
0
0
1000
Time (s)
D
×10^3
6
0.003
0.005
0.004
Opn1mw^R
rd/rd cl
Opn4^-/-
Periodogram value
0
0
0.03
Frequency (Hz)
E
0.15
Frequency (Hz)
0
*
****
*
**
dLGN
vLGN
OPN
F
60
% of infra-slow oscill. cells
0
***
*
****
dLGN
vLGN
OPN
fast oscillatory activity
G
0.4
% PSD
0
41
27
20
60
Frequency (Hz)
H
50
Frequency (Hz)
0
*
****
dLGN
vLGN
OPN
I
60
% of fast oscill. cells
0
*
***
****
dLGN
vLGN
OPN

# Fig. 5

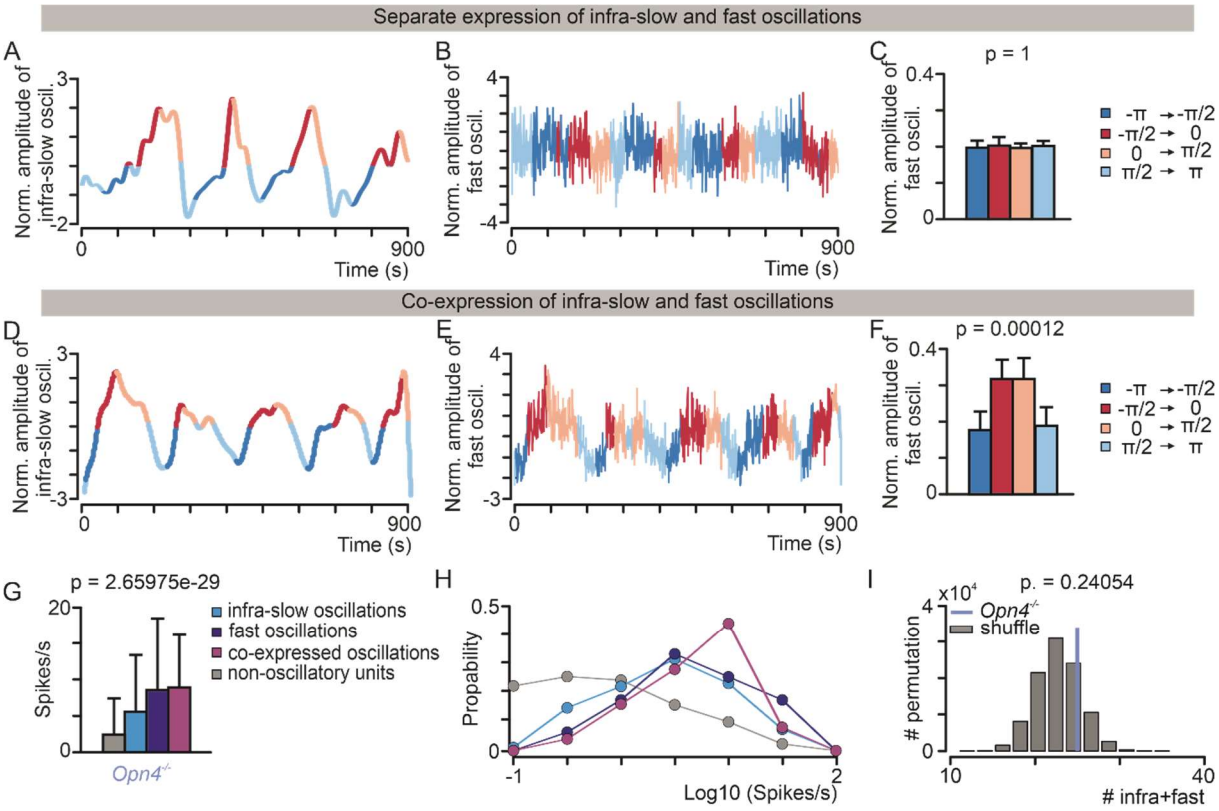
Separate expression of infra-slow and fast oscillations
A
Norm. amplitude of infra-slow oscil.
Time (s)
B
Norm. amplitude of fast oscil.
Time (s)
C
p = 1
Norm. amplitude of fast oscil.
-π → -π/2
-π/2 → 0
0 → π/2
π/2 → π
Co-expression of infra-slow and fast oscillations
D
Norm. amplitude of infra-slow oscil.
Time (s)
E
Norm. amplitude of fast oscil.
Time (s)
F
p = 0.00012
Norm. amplitude of fast oscil.
-π → -π/2
-π/2 → 0
0 → π/2
π/2 → π
G
p = 2.65975e-29
Spikes/s
infra-slow oscillations
fast oscillations
co-expressed oscillations
non-oscillatory units
Opn4-/-
H
Propability
Log10 (Spikes/s)
I
p. = 0.24054
x10^4
Opn4-/-
shuffle
# permutation
# infra+fast

# Fig. 6